

Effective stress regime around a jacked steel pile during installation, ageing and load testing in chalk

Buckley, R.M.¹, roisin.buckley13@imperial.ac.uk

Jardine, R.J.¹,

Kontoe, S.¹,

Lehane, B.M.²

1. Department of Civil & Environmental Engineering, Imperial College London, UK 2. School of Civil Engineering, Univ. of Western Australia, Perth

ABSTRACT

This paper reports experiments with 102mm diameter closed-ended instrumented Imperial College Piles (ICPs) jacked into low to medium density chalk at a well characterised UK test site. The 'ICP' instruments allowed the effective stress regime surrounding the pile shaft to be tracked during pile installation, equalisation periods of up to 2.5 months, and load testing under static tension and one-way axial cyclic loading. Installation resistances are shown to be dominated by the pile tip loads. Low installation shaft stresses and radial effective stresses were measured that correlated with local CPT cone resistances. Marked shaft total stress reductions and steep stress gradients are demonstrated in the vicinity of the pile tip. The local interface shaft effective stress paths developed during static and cyclic loading displayed trends that resemble those seen in comparable tests in sands. Shaft failure followed the Coulomb law and constrained interface dilation was apparent as the pile experienced drained loading to failure, although with a lesser degree of radial expansion than with sands. Radial effective stresses were also found to fall with time after installation, leading to reductions in shaft capacity as proven by subsequent static tension testing. The jacked, closed-ended, piles' ageing trends contrast sharply with those found with open piles driven at the same site, indicating that ageing is affected by pile tip geometry and/or installation method.

Keywords: chalk, piles, shaft capacity, time effects, effective stresses

1 INTRODUCTION

2 Extensive deposits of chalk exist across Northern Europe, the North and Baltic Seas, where thicknesses
3 can exceed 1200m (Clayton *et al.*, 2002). Chalk, a variable calcium carbonate soft rock which
4 frequently includes hard siliceous “flint” nodules (Clayton, 1986) is classified by its fabric grade and
5 intact dry density. Intact Unconfined Compressive Strength (UCS) tests on saturated samples give
6 ranges from approximately 1.25 to greater than 12.5MPa (Bowden *et al.*, 2002) and cone tip
7 resistances, q_c from 4 to greater than 50MPa (Power, 1982). High porosity chalk is known to degrade
8 rapidly through a putrefaction mechanism when subjected to percussive pile driving (Hobbs and
9 Atkinson, 1993, Lord *et al.*, 2002), high amplitude laboratory cyclic simple shear testing (Carrington *et*
10 *al.*, 2011) or cyclic cone penetration tests (Diambra *et al.*, 2014). Chalk’s sensitivity, which relates to
11 its lightly cemented structure and crushable calcium carbonate particles is thought to be responsible
12 for the remarkably low ultimate unit shaft resistances, indicated for driven piles by the sparse data set
13 of published loading tests.

14 Lord *et al.* (1994) and Lord *et al.* (2002)’s design guidance indicates ultimate shaft resistances of 20
15 and 120kPa for preformed piles driven in low-medium and high density chalk respectively. The latter
16 appear very low given the chalk’s UCS and q_c ranges. The need to optimise designs for multiple
17 offshore high value wind-farm applications prompted a Joint Industry Project (JIP) to investigate, for
18 tubular steel piles driven in low-medium density chinks: i) the fundamental, effective stress,
19 mechanisms behind the low shaft resistance mobilised during installation ii) any potential changes in
20 pile capacity with time and iii) the effect of axial cyclic loading on aged pile capacity. Full scale dynamic,
21 static and cyclic field testing conducted in water depths of up to 42m as part of the Wiking German
22 Baltic Sea offshore wind project form another part of the research that is described by Barbosa *et al.*
23 (2015) and Jardine (2018). Six 1.37m diameter steel tubular piles were driven and tested at three
24 locations, where chalk is overlain by variable thicknesses of glacial deposits. Both low driving
25 resistances and strong beneficial ageing trends were demonstrated that led to long term shaft

26 resistances far higher than currently recommended design values. Buckley *et al.* (2017) report another
27 JIP element that investigated systematically the effects of ageing and cyclic loading on multiple
28 139mm Outside Diameter (OD) open steel tubes driven in low-medium density chalk at an onshore
29 site near St. Nicholas at Wade, Kent, SE England, finding: (i) low local installation shaft resistances that
30 were comparable to those observed at Wikinger and depended strongly on the relative depth (h) of
31 the pile tip; (ii) average tension shaft capacities increasing markedly, over time, following a hyperbolic
32 trend, to reach after 8 months values 5.3 times greater than the (compressive) End of Driving (EoD)
33 resistances and 4.3 times higher than the CIRIA 20kPa value (iii) a remoulded and reconsolidated
34 annulus of chalk surrounding the pile shaft with void ratios falling around 23% below the undisturbed
35 values. Re-consolidation of chalk putty and subsequent increases in radial effective stresses were
36 thought to have contributed to the piles' ageing behaviour, potentially along with redox reactions and
37 re-cementing in the chalk. One-way axial cycling, imposed at around 250 days after driving, led to
38 responses that ranged from stable to unstable, depending on the loading parameters. While the aged
39 and previously untested piles' capacities were not sensitive to one-way axial cycling for the considered
40 loading levels and number of cycles, significant permanent displacements could develop under
41 relatively modest cyclic loading levels. High level two-way cycling could also prove more damaging.

42 The above driven pile tests represent a systematic investigation into ageing and cyclic loading in chalk.
43 However, the piles did not carry local instrumentation that could track the fundamental processes
44 that govern their installation, ageing, static and cyclic loading responses. A separate programme of
45 highly instrumented Imperial College Pile (ICP) tests was carried out to explore these aspects at the
46 same test site, leading to the observations set out in this paper regarding the shaft effective stress
47 regime during installation, long term equalisation and load testing.

48 The 102mm OD steel ICP piles' are, as described by Bond *et al.* (1991), equipped to measure local
49 radial and shear stresses on their shafts as well as pore pressures, shaft axial loads and temperatures.
50 ICP experiments have advanced fundamental understanding of displacement pile behaviour in sands

51 and clays (Bond, 1989, Lehane, 1992, Chow, 1997) that led to improved, physically reasonable driven
52 pile design methods (Lehane *et al.*, 1993, Jardine *et al.*, 2005, Lehane *et al.*, 2005). However, the
53 valuable insights could only be gained by accepting jacked installation and a closed-ended
54 configuration that may not always be representative of industrial piling. It has not been possible, to
55 date, to devise local stress sensors that can function as reliably on driven open pipe-piles.

56 **SITE CONDITIONS**

57 The tests were conducted in a chalk quarry close to St. Nicholas at Wade, approximately 15km west
58 of Margate in the UK County of Kent (UK Grid: TR 25419 66879), where earlier sampling and *in situ*
59 testing studies have taken place, as well as programmes of (static and cyclic) lateral tests followed by
60 axial cyclic loading (SETech, 2007, Fugro, 2012b, a, Dührkop *et al.*, 2015, Ciavaglia *et al.*, 2017). Figure
61 1 shows the overall layout including the current Imperial College test area. Buckley *et al.* (2017) outline
62 the site characterisation, which included multiple cone penetration tests with pore pressure
63 measurement (PCPT) and laboratory testing. The laboratory tests were conducted on samples taken
64 from the adjacent earlier JIP site (Figure 1). Further PCPT and seismic CPT (SCPT) have been performed
65 recently to aid the ICP experiments' interpretation.

66 The overburden and weathered chalk has been removed at the quarry, leaving chalk from the Margate
67 White Chalk subgroup. Intact Dry Density (IDD) ranges from 1.38 to 1.54 Mg/m³, indicative of a low
68 density chalk (Bowden *et al.*, 2002), although a layer with IDD up to 1.64 Mg/m³ was encountered
69 between 2.9 and 3.3 mbgl. The water table is reported 11.6 mbgl below the current quarry base, but
70 the degree of saturation remains between 90 and 100% up to ground level. Chalk specimens crushed
71 from quarry samples indicate predominantly silt sized grains, see Figure 2 after Bialowas *et al.* (2016)
72 and Chan (2017). The median grain size, D₅₀ for crushed chalk samples tends to vary with the method
73 of sample preparation and grinding (Bundy, 2013). Intact chalk is known to be markedly brittle (Jardine
74 *et al.*, 1984); Lord *et al.* (2002) indicate that c' can range from 100kPa to > 2MPa with $36^\circ < \varphi' < 42^\circ$.
75 For remoulded chalk, c' falls between 0 and 10kPa with $29^\circ < \varphi' < 34^\circ$. Consolidated drained triaxial

76 tests on intact quarry samples showed best fit $c' = 387\text{kPa}$ and $\varphi' = 41^\circ$. Remoulded samples tested
 77 under undrained triaxial compression showed peak φ' angles around 37.5° , assuming zero cohesion.
 78 Ring shear interface tests by the Authors in the Bishop apparatus, using mild steel interfaces to
 79 represent field pile roughness (average roughness, $R_a \approx 10\text{-}15\mu\text{m}$) values, indicate residual δ_r' angles
 80 between 30 and 31° , similar to those reported by Le *et al.* (2014) and Ziogos *et al.* (2016). Bishop ring
 81 shear tests carried out by Chen (2017), on samples from the test site, indicated δ_r' angles of between
 82 26 and 31.5° (depending on normal effective stress level) using stainless steel interfaces prepared with
 83 roughness, R_a of $1.22\ \mu\text{m}$, similar to those of industrial CPT friction sleeves.

84 Details of the CPT q_c and sleeve friction, f_s measured close to the jacked ICP piles are shown in Figure
 85 3, over the limited depths of penetration, along with G_{hV} values from cross hole seismic surveys,
 86 seismic CPT G_{vh} measurements, and the site profile from borehole logs. Also shown on this Figure are
 87 the PCPT penetration pore pressures measured at both the tip (u_1) and shoulder (u_2) positions. PCPT
 88 q_c ranges from 10 to 20MPa while sleeve friction, f_s , lies between 100 and 500kPa . The penetration
 89 pore pressures are remarkably high across the site, reaching 7.8MPa within the depth of interest at
 90 the u_1 position and 4.9MPa at the u_2 position. Cone resistance varied laterally, with local spikes up to
 91 60MPa which reflect thin flint bands. Dissipation tests with 43.8mm diameter (D) piezocones showed
 92 50% dissipation after 4 to 13 seconds at the u_2 position, indicating horizontal consolidation
 93 coefficients, $c_{h,\text{piezo}}$ of $\approx 1 \times 10^{-3}\ \text{m}^2/\text{s}$, assuming high rigidity indices in the surrounding intact chalk
 94 and applying the approach of Teh and Houlsby (1991). The degree of pore pressure dissipation during
 95 CPT penetration can be assessed using a normalised velocity, V (Finnie and Randolph, 1994) defined
 96 as:

$$V = \frac{vD}{c_h} \quad \text{Eq. 1}$$

97 Where the standard tip velocity, v is 20mm/s . The critical values of V depend on which method is used
 98 to define c_h , as the normally consolidated values seen in oedometer tests ($c_{h,NC}$) fall well below
 99 $c_{h,\text{piezo}}$ which in turn falls below those applicable in lightly overconsolidated states, $c_{h,OC}$. Centrifuge

100 tests indicate a transition to fully undrained conditions at V values of between 10 and 100 when $c_{h,NC}$
101 is substituted (Finnie and Randolph, 1994, Randolph, 2004, Cassidy, 2012, Suzuki, 2014). If $c_{h,piezo}$ is
102 considered $\approx 5 c_{h,NC}$ (Fahey and Lee Goh, 1995) for the chalk tests, the transition range reduces to 2
103 and 20. The CPT penetration corresponds to a normalised velocity, $V \approx 0.8$, indicating that partially
104 drained conditions apply. Assuming the cone end bearing failure mechanism extends approximately
105 2D below its tip leads to similar conclusions; the dissipation tests also indicate $40 \pm 15\%$ pore pressure
106 dissipation in the 3.6 seconds required for the pile tip to pass through its earlier failure zone.

107 **IMPERIAL COLLEGE PILE**

108 The closed ended 102mm diameter Imperial College Piles' (ICP) main shaft sections are tubular with a
109 9.5mm wall thickness. With the exception of their stainless steel Surface Stress Transducer (SST)
110 sections, the piles are made from molybdenum steel and had typical average roughness (R_a) of $\approx 5\mu\text{m}$
111 at the time of installation. High axial loads were expected in chalk and the dual instrument clusters
112 adopted were identical to the higher capacity cells employed by Chow (1997). They are distinguished
113 in Figure 4 by their *leading* and *following* positions, as defined by their ratios of, h , height above the
114 pile tip, normalised by the pile radius, R . Each includes an axial load cell (ALC), two pore pressure
115 transducers (PPT) and an SST, which measures radial total stress, σ_r and shear stress, τ_{rz} on the pile
116 surface, as well as temperature. The instruments' design, development and calibration procedures are
117 described by Bond *et al.* (1991). The ALCs, which are insensitive to radial stress and have a nominal
118 capacity of 405kN at 0.2% axial strain, were calibrated against known forces in the laboratory. The
119 pore pressure transducers, housed in holders integrated with the ALCs, were saturated with silicone
120 oil in the laboratory and transported sealed prior to installation on site. The SSTs were calibrated in a
121 jig that could apply radial and shear stresses directly and assess the cells' cross sensitivities related to
122 the effects of i) axial load on the radial and shear strain gauge output ii) shear stress on the radial
123 strain gauge output iii) radial stress on the shear strain gauge output and iv) the effect of temperature
124 changes on all the gauges. The radial total stress measurements are accurate to typically $\pm 3\text{kPa}$ and

125 the shear stress measurements to typically $\pm 1.5\text{kPa}$. Calibrations were conducted at University of
126 Western Australia prior to their return to the UK. Further calibrations were conducted at Imperial
127 College and Cambridge *in situ* Ltd. after repair work conducted during and shortly after the test
128 programme.

129 Bond *et al.* (1991) recognised the SSTs' asymmetric design makes them susceptible to bending under
130 high axial load. This was not unduly significant at the initial clay and loose sand test sites, where end
131 bearing and overall axial loads were relatively low. However, Chow (1997) found that installation and
132 compression load testing led to far greater tip and overall axial loads in dense marine sand that caused
133 the SSTs to deflect and under-register both σ_r and τ_{rz} . High end bearing loads were anticipated for,
134 and experienced in, the chalk tests that would lead to stress under-registration when the pile was
135 penetrating downwards, but have no effect when the pile head load was zero, negative and relatively
136 low, as in tension tests. Instrument malfunctions can occur during field testing. However, the ICP
137 configuration includes redundancy that allows cross checking and error identification. Local τ_{rz} can be
138 related to average shear stresses interpolated between the ALCs and σ'_r can be checked for
139 consistency with laboratory interface shear tests. The dual radial sensor circuits and pore pressure
140 transducers available in each cluster provide back-up that proved useful in the chalk experiments.

141 **TESTING PROGRAMME**

142 As summarised in Table 1, the testing programme began in October 2015 and was completed in
143 February 2016. The piles were assembled on site using threaded casings, sealed with "O" rings, to give
144 total lengths of between 4.1 and 4.3m. To avoid overloading the ALCs under the high end bearing
145 loads anticipated, the piles were installed from a free depth, 1.6m below current ground level, through
146 150mm diameter PVC liners placed in a backfilled trial pit. This resulted in embedded lengths of
147 between 2.5 and 2.7m ($L/D = 24.5$ to 26.5). The pile end conditions differed between tests; ICP01 was
148 installed with a flat closed-end and ICP02 utilised a 60° conical tip to aid penetration if flint nodules
149 were encountered, resulting in h/R values that differ slightly between tests (Figure 4). The leading

150 ALCs were located above the pile tips and recorded the base loads plus minor contributions from the
151 short (≈ 87 and 150mm) lengths of shaft below the base ALCs.

152 **TESTING PROCEDURES**

153 *Pile Installation*

154 The piles were installed by jacking against a 30t CPT truck equipped with a 270kN hydraulic ram.
155 Installation took place under displacement control, at jacking rates which varied unavoidably, but
156 averaged at 4.8mm/s and 3.4mm/s for ICP01 and ICP02 respectively, with 50mm strokes separated by
157 60 to 90 second zero-load pauses. The latter were chosen to ensure a similar degree of cyclic loading
158 to that experienced by open piles driven by the Authors at the same site, which had penetrated by
159 around 50mm per blow. Installation force was measured by a load cell at the pile head or by the CPT
160 truck's systems. All instruments were logged at 1 to 2 second intervals during installation. The process
161 was not fully continuous. Apart from the intervals imposed between strokes, adding extra casing
162 lengths led to total installation times of 80 to 124 minutes per pile, while only 4 to 15 minutes were
163 required for the driven piles reported in Buckley *et al.* (2017). The ICPs inevitably experienced greater
164 excess pore pressure dissipation during installation.

165 *Equalisation and long term monitoring*

166 The instruments were monitored over the weeks following installation with readings every 5 minutes
167 over ageing periods of 23 and 80 days that represent the longest duration ICP tests to date. The
168 instruments were powered continuously over the relatively cold and wet 2015/16 winter, apart from
169 four unintended short supply breaks. Instrument drifts (change in voltage output under zero load)
170 were anticipated and the results were corrected by comparing instrument 'zero-values' established
171 before and after each experiment, assuming constant drift rates between installation and extraction.

172 *Load testing*

173 The two ICPs were subjected to tension testing after their ageing monitoring periods using the
174 equipment shown in Figure 5, designed and built at Imperial College, that transferred reaction loads
175 to railway sleeper mat foundations. Tension loading avoided high axial loads that might overload the
176 ALCs or cause SST measurement errors. Axial load was measured by an annular load cell and was
177 applied by both electric and manual hydraulic pumps through a hollow ram. Displacement was
178 measured using three LVDTs spaced circumferentially around the pile, supported on retort stands
179 placed around 1m from the pile axis. Loads were applied in increments of $\approx 10\%$ of the failure load and
180 held for 10 minute creep periods. The test failure criterion was set as either: i) a displacement of 10%
181 of the pile diameter ii) a semi-logarithmic creep rate, k_s of 0.2mm/log cycle of time or iii) a load equal
182 to the safe limit of the testing system. Following each tension failure, the piles were unloaded to a
183 small tensile load to retain system stability and 20 to 21 relatively high-level one way tension cycles
184 were applied. The cycles were load controlled at 0.016Hz following the square wave pattern illustrated
185 in Figure 6, which also defines the loading parameters. All instruments were logged every 1 to 2
186 seconds.

187 **RESULTS & INTERPRETATION**

188 *Installation resistance*

189 The total axial forces, Q_{tot} measured during penetration strokes are shown on Figure 7, along with the
190 forces measured at the pile base, Q_b , the average shaft stresses, τ_{avg} (calculated as Q_{tot} less Q_b over
191 the total shaft area) and the envelope of q_c measurements. The lowermost load cell (ALC1)
192 measurements include contributions from short lower sections of shaft, for which the Q_b traces have
193 been corrected by assuming that PCPT sleeve friction values (measured at $h/R \approx 5.5$) apply near the
194 base. This assumption is considered reasonable since similar shear stresses (up to 280kPa) applied
195 along these shaft lengths during static tension testing, as discussed later.

196 Axial loads up to 270kN developed during installation pushes, comparable to those in Chow's (1997)
197 dense sand tests at Dunkirk. The base resistance Q_b comprised $\approx 80\%$ of the head load, Q_{tot} , as in
198 Chow's tests and with other piles jacked into weathered chalk (Hodges and Pink, 1971). Lower tip
199 resistance contributions develop in clays, where Q_b typically comprises $< 20\%$ of the total (Lehane,
200 1992, Lehane and Jardine, 1992, Chow, 1997). As mentioned earlier, PCPT tests identified laterally
201 discontinuous, thin, high resistance flint bands. Figure 7 shows that τ_{avg} was highest in a layer
202 between 2 and 2.3m, but fell in both tests to approximately 50kPa as the tips penetrated to greater
203 depths. While the overall average shaft resistance of 50kPa exceeds the CIRIA driven pile static
204 capacity recommendation of Lord *et al.* (2002), the average shear stresses recorded over the main
205 shaft lengths, between ALC1 and the pile top, were on average 11kPa, falling well below both the
206 average calculated over the whole pile length (seen on Figure 7) and the CIRIA guideline value. Small
207 residual ALC1 loads (typically $< 3\text{kN}$) remained after unloading at the end of each jacking push, whose
208 distributions with depth mirrored the profiles of τ_{avg} . We also recall from Buckley *et al.* (2017) that
209 open-ended driven piles developed average shaft resistances of 16kPa on installation at the same site,
210 20% below the CIRIA recommended value and the ICP test mean of 50kPa.

211 *Penetration pore pressures*

212 Pore pressure measurements were taken high above the water table, where the ambient pore water
213 pressures are likely to depend on infiltration rates and permeability gradients. Negative pressures
214 could be expected under dry conditions, but small positive values appeared to operate over the
215 2015/16 winter. The penetration pore pressures are shown on Figure 8, along with the measurements
216 made during PCPT penetration, plotted in this instance against h/R where h is the distance from the
217 pile or PCPT tip and R is the pile or PCPT radius. Low, typically $< 10\text{kPa}$, penetration pore pressures
218 were measured by the pile sensors located between 0.25 and 1.76m behind the pile tip, while values
219 exceeding 4MPa were measured at the PCPT u_2 position $\approx 38\text{mm}$ from the cone tip reaching as high as
220 7.8MPa at the tip (u_1). The piles were installed under displacement control at variable jacking rates,

221 which are equivalent to normalised velocities V of between 0.33 and 0.46, well below the minimum
222 of 2 to 20 proposed earlier for undrained conditions. Strong gradients of pore pressure with distance
223 from the pile base are indicated in Figure 8, to which the piles' partially drained tip conditions
224 contributed. Effectively drained conditions applied over most of the shaft above the tip, due to the
225 reduced total stresses (as described later) and additional dissipation of pore pressures over the time
226 taken for the upper shaft sections to reach any given chalk horizon. Partially drained pore pressure
227 distributions were also assessed by Buckley *et al.* (2017) along the shafts of tubular piles driven at the
228 same site, although their degrees of dissipation would have been lower, as the driven piles had larger
229 diameters and shorter total installation times.

230 *Base resistance measurements*

231 The closed-ended ICP end bearing load profiles shown on Figure 7 have similar forms to the q_c profiles
232 with the exception of the higher pile tip resistance band encountered between 1.9 and 2.3m. Given
233 their geometric similarities, it is reasonable to expect the closed-end bearing pressures q_b , corrected
234 for the shaft contribution as described earlier, to correlate with the net cone tip resistance q_t , where
235 $q_t = q_c + u_2(1 - a)$ and a is the cone area ratio. For deep penetration $q_b = \alpha q_t$ (Baligh, 1985,
236 Randolph *et al.*, 1994) where α depends on penetration rate and pile-end geometry. Jacking under
237 partially drained or drained conditions is known to increase tip resistance (Chung *et al.*, 2006), while
238 positive rate effects apply under undrained conditions. The variable installation rates and geometries
239 of the jacked piles results in α values between 1.0 and 1.6. Figure 9 shows the variation of α with non-
240 dimensional velocity V (defined in Eq. 1 and applying over an installation push for the pile) for the pile
241 and PCPT, indicating the general trend for q_b/q_c to reduce with V and the limits for installation under
242 drained or partially drained conditions. The relative scatter in this plot is probably attributable to the
243 correction of the base measurements with the sleeve friction values described above. The parameter
244 α can be seen to reduce with increasing V tending towards an α value of 1 at $V_{pile} = V_{cpt}$. Installation
245 end bearing appears to be controlled by pile tip q_t and the degree of local drainage.

246 *Shaft effective stresses close to pile tips*

247 It has been argued that closed-ended piles develop triaxial compression failure zones immediately
248 beneath their tips during penetration (Yang *et al.*, 2010). The average vertical stress, $\sigma_z (= \sigma_1)$ should
249 then equal q_t (or q_b) beneath the tip, with $\sigma_1 = q_t = \sigma'_z + u_1$, where u_1 is the average pore pressure
250 over the cone tip. Applying the argument presented by Jardine *et al.* (2013) for sand, the maximum
251 moving radial effective stresses, σ'_{rm} applying immediately below the pile tip during rapid penetration
252 can be calculated from the Mohr Coulomb failure criterion for triaxial compression; $\sigma'_{rm} =$
253 $\tan^2(45 - \varphi'/2)\sigma'_z - 2c'\tan(45 - \varphi'/2)$ where peak $\varphi' = 41^\circ$ for intact chalk, and σ'_z beneath the
254 tip = $q_t - u_1$. The mean u_1 pore pressures, shown in Figure 8, give $u_1 \approx 0.4q_t$, leading to $\sigma'_{rm} \approx$
255 $0.125q_t - 2c'\tan(45 - 41/2)$ beneath the pile tip during steady penetration. Taking $c' = 387\text{kPa}$
256 gives $900 < \sigma'_{rm} < 2150\text{kPa}$ on the pile axis at the tip ($h=0$). Moving to slightly higher locations, the CPT
257 sleeve resistance values, f_s indicate “moving” effective stresses almost an order of magnitude lower,
258 calculated from $\sigma'_{rm} = f_s/\tan\delta'$ by applying the measured interface shear angle, $\delta'_{cpt} = 30.5^\circ$, giving
259 $100 < \sigma'_{rm} < 350\text{ kPa}$ at $h/R = 5.5$. The value of $\delta'_{cpt} = 30.5^\circ$ was chosen based on the results of
260 interface ring shear tests on stainless steel interfaces with similar roughness to the CPT cone sleeves
261 at a confining stress of 200kPa , compatible with the mean f_s value (Chan, 2017). The near pile tip values
262 of σ'_{rm} discussed above are compared below to the local radial effective and shear stresses measured
263 at the SST locations measured higher up the pile shaft.

264 *Local shaft effective stresses*

265 Figure 10 shows the stationary radial effective, σ'_{rs} and stationary τ_{rz} stresses measured at the
266 *leading* instrument during both ICP tests; the following instrument data are discussed later. The
267 stationary stresses are free of the bending effects mentioned previously. Since the pile was installed
268 under partially drained conditions and the stresses equalised rapidly after each stroke, σ'_{rs} can be
269 considered equivalent to the equilibrium values applying shortly after installation to the same tip
270 depth. The σ'_{rs} values were similarly low in both tests, varying from ≈ 20 to 60kPa , far below the values

271 discussed above for the pile tip region. When the piles were stationary, the measured SSTs manifested
272 low negative τ_{rz} values, reflecting the shafts' tendency to resist locked-in toe forces when the head
273 load was removed.

274 The *leading* SSTs profiles of σ'_{rs} correlate directly with the CPT q_t -depth trends (see Figure 11), as has
275 been noted previously for sands (Lehane, 1992, Chow, 1997) and incorporated into CPT pile design
276 methods (Jardine *et al.*, 2005, Lehane *et al.*, 2005). The σ'_{rs} - q_t trends for ICP01, which had a flat
277 bottomed end, exhibit a higher degree of scatter than those for ICP02, which utilised a conical tip. The
278 average q_t/σ'_{rs} ratio is approximately 405 at the *leading* instrument. The stationary radial stresses
279 applying further along the shaft are shown on Figure 12a, where σ'_{rs} is normalised by q_t and plotted
280 against h/R for the last 500mm of penetration in each test. Also shown on this plot are trends observed
281 in loose silica sand at Labenne (Lehane, 1992, Lehane *et al.*, 1993), dense Dunkirk sand (Chow, 1997)
282 and uncemented calcareous sand (Lehane *et al.*, 2012). The σ'_{rs}/q_t ratios can be seen to fall well
283 below the measurements made at Labenne and Dunkirk and closer to the calcareous sand trend. Only
284 slight reductions in normalised σ'_{rs}/q_t were observed between the *leading* instrument ($h/R = 8 - 8.4$)
285 and the *following* cluster ($h/R = 31.9 - 32.4$), suggesting that the extreme stress reduction that takes
286 place between the pile tip and the shaft develops over a short h/R range.

287 Further evidence is presented in Figure 12b by adding to the stationary SST measurements i) "moving"
288 radial effective stresses inferred from PCPT f_s traces and ii) profiles of τ_{rz} found from back analysis of
289 dynamic tests on piles driven at the site; Buckley *et al.* (2017). The three sources of evidence all point
290 to low local shear resistances over the majority of the shaft and markedly higher resistances closer to
291 the pile tip. Ciavaglia *et al.* (2017) report a similar trend from their analysis of strain gauge
292 measurements on open piles driven at the same site; shaft resistances four to six times higher applied
293 on the lower half of their 762mm diameter piles which were driven to 4m embedment.

294 *Long term equalisation*

295 Continuous monitoring tracked the variations between installation and final load testing in local shaft
296 effective stresses. The trends for pore pressure, radial effective stress and shear stress over the first
297 10 minutes after the final jack push are shown on Figure 13, while the long term σ'_{rs} trends are plotted
298 against logarithm of time on Figure 14. Only small excess pore pressures were seen that dissipated
299 quickly and remained relatively stable at <4kPa.

300 The ICP01 pile's radial effective shaft stresses fell by 11 to 26% over its 23 days ageing period, while
301 ICP02's fell by 29 to 34% over 80 days. Radial total stress reductions dominated, although some
302 discrete pore pressure peaks were observed that correlated with recorded rainfall events (Met-Office,
303 2016). Residual ALC1 loads of between 11.8 and 16.7kN were measured at the ends of installation for
304 ICP01 and ICP02 respectively, which reduced to 3.7kN and 2kN at the end of the equalisation. The SST
305 τ_{rz} values were negative at the end of jacking and reduced towards zero over the monitoring periods.

306 *Static Load testing*

307 The two piles were subjected to stage-loaded tension testing after ageing and full re-consolidation of
308 any chalk putty to a lower water content (see Buckley *et al.*, 2017), giving the net load-displacement
309 curves presented in Figure 15, where the net load is the tension load less the pile self-weight. The final
310 static holding periods in both tests were ≥ 30 minutes. Pile ICP01 underwent minor axial realignment
311 at low loads and showed a slightly softer initial response than ICP02. The piles' failures were identified
312 from their displacement creep trends under constant load. In both cases the piles failed when the
313 displacement exceeded creep rates of 0.2mm/log cycle of time, reaching their peak loads after pile
314 head displacements of 1.43 and 2.58mm.

315 The axial loads measured along the pile length at failure, shown on Figure 16, indicate failure loads of
316 $\approx 9 \pm 1$ kN at the ALC1 position. Given that drained conditions applied, and so no reverse end bearing
317 could develop, the ALC1 loads imply local shear stresses of between 200 and 280kPa along the final
318 section of the shaft positioned below this load cell, similar to the PCPT sleeve friction measurements

319 described previously. These values far exceed the CIRIA 20kPa recommendation. However, the ALC
 320 measurements indicate significantly lower average stresses applied further along the pile shaft,
 321 leading to an average of 22kPa, which is similar to both the shaft stresses seen during installation and
 322 the current CIRIA recommendation for ultimate shaft resistance of 20kPa. We note again that open-
 323 ended driven piles at the same site developed far higher long-term shaft resistances of 87kPa (Buckley
 324 *et al.*, 2017).

325 The ICP tests provided a unique opportunity to observe how the local effective stresses respond during
 326 load testing. The effective stress paths measured at the instrument clusters during one way static
 327 loading are presented on Figure 17, where the τ_{rz} axis is negative under tension loading. The radial
 328 effective stresses increased during loading, as seen previously in sands and interpreted as constrained
 329 dilation at the interface (Lehane *et al.*, 1993, Chow, 1997). The shear and effective stresses mobilised
 330 at failure, τ_f and σ'_{rf} respectively show peak stress ratios $\delta_f (= \tan^{-1}(\tau_f / \sigma'_{rf}))$ close to the δ'_{cv} angles
 331 seen in interface ring shear tests on samples from the site. It appears that ultimate shaft shear stress
 332 can be described by a Coulomb expression, similar to that proposed for sands (Lehane *et al.*, 1993)
 333 where:

$$\tau_f = (\sigma'_{rc} + \Delta\sigma'_{rd})\tan\delta'_{cv} \quad \text{Eq. 2}$$

334 And σ'_{rc} is the equalised radial effective stress, $\Delta\sigma'_{rd}$ is the change in radial effective stress during
 335 loading due to constrained dilation in the interface or any new shear band that forms and δ'_{cv} is the
 336 constant volume interface friction angle. Boulon and Foray (1986) showed that with sands, the
 337 magnitude of $\Delta\sigma'_{rd}$ can be estimated by a simple cavity expansion expression:

$$\Delta\sigma'_{rd} = \frac{2G\Delta r}{R} \quad \text{Eq. 3}$$

338 The G value in Eq. 3 should ideally be measured in the G_{hh} direction and may need to account for fabric,
 339 void ratio, strain level and stiffness non-linearity. The Δr term may be taken as $2R_a$ for sands in cases
 340 where the interface's relative roughness, R_n ($R_n = R_a/D_{50}$) is less than the critical value, which for a
 341 perfectly rough response is approximately 0.1 (Kishida and Uesugi, 1987, Lings and Dietz, 2005). Figure

342 2 indicates that the chalk's D_{50} is between ≈ 3.0 and $6.0 \mu\text{m}$, giving $R_n \approx 0.8$ to 1.7 , and so far exceeding
343 the perfectly rough limiting value. The SST sensors indicated $\Delta\sigma'_{rd}$ from ≈ 11 to 14kPa , in three cases
344 and 96kPa in one isolated case. Locally instrumented triaxial tests on intact and reconsolidated chalk
345 by Jardine *et al.* (1984) and Doughty (2016) showed that the behaviour is likely to be principally elastic
346 in most of the soil mass over the implied strain range. The undisturbed *in situ* seismic G_{hh} values shown
347 in Figure 3 range from ≈ 400 to 1200MPa . However, locally lower G values may apply close to the shaft
348 due to installation effects and re-consolidation. Multi-stage resonant column tests on samples taken
349 from the site carried out by Fugro (2012a) indicated G_{vh} of 250 to 300MPa at the appropriate mean
350 effective stress level for remoulded chalk. Substituting G ranges of 250 to 1200kPa into Eq. 3 allows
351 us to estimate Δr for these tests as falling mostly between 0.23 and $2.04 \mu\text{m}$, with one isolated high
352 value of $9.8 \mu\text{m}$. The resulting Δr values fall well below the piles' surface average peak-to-trough
353 roughness value.

354 *Change in static capacity with time*

355 The trends with time in static shaft capacity can be gauged most easily by comparing i) the shaft shear
356 stresses mobilised at tension failure $\tau_{s,(t)}$ with ii) the average (positive compressive) shear stress,
357 $\tau_{s,EoJ}$ measured during the final jacking stroke (Figure 7). The installation stresses are higher and,
358 neglecting any influences of displacement rate and variation in capacity with loading direction, shaft
359 capacity reduced over time by 20% for ICP01 and 18% for ICP02. These losses are compatible with,
360 although less marked than, the local radial effective stress trends presented in Figure 14.

361 The jacked, closed-ended, piles' ageing behaviours contrast strongly with those seen in parallel tests
362 at the same site on open ended driven piles reported by Buckley *et al.* (2017), whose hyperbolic trend
363 curve indicated gains of 327 and 448% over 23 and 80 days respectively, building to 530% after 250
364 days (see Figure 18), similar to the trend reported by Ciavaglia *et al.* (2017) for 762mm diameter piles
365 installed at the same site. For the driven piles, the average tensile shaft capacity along the pile length,
366 $\tau_{s,(t)}$ from the static tension test is compared with the end of driving compressive shaft capacity from

367 the dynamic test, $\tau_{s,EOD}$, assuming that tensile and compressive shaft capacity are similar, even if not
368 exactly equal. While dynamic pile tests are subjected to more uncertainty than static tension load
369 tests, the trend shown on Figure 18 indicates that the static tensile shaft resistance more than doubled
370 between the 10 and 106 test ages, consistent with the indicated overall capacity trend increase. The
371 set-down shown by the jacked piles also contrasts sharply with the marked set-up seen in the Wikinger
372 full-scale offshore tests described by Barbosa *et al.* (2015) and Jardine (2018).

373 The different behaviours of driven open-ended and slowly jacked closed-ended piles requires further
374 investigation. Buckley *et al.* (2017) propose a mechanism involving consolidation of the chalk putty
375 annulus formed around the open pile and long-term radial stress growth post driving to explain the
376 driven piles' strong set-up, while noting that redox reactions between the pile shaft and re-cementing
377 of the puttyfied chalk could also be influential. The lack of set-up shown by the (mainly oxidisable
378 molybdenum steel) jacked piles indicates that physiochemical effects and re-cementing cannot be the
379 dominant ageing mechanism. The two types of piles were installed into chalk of the same grade and
380 density and allowed to equalise over similar time periods prior to failing under the same testing
381 procedure, so the different ageing trends must originate in either i) the ICP's closed ends and/or ii)
382 the piles' modes and rates of installation. The driven piles penetrated one to two orders of magnitude
383 more rapidly than the ICPs. Also, no evidence was seen on extraction of the ICPs of any previously
384 puttyfied zone, as was found adhering to the driven piles.

385 *Cyclic loading*

386 Limited packages of one-way axial cyclic loading were applied after the ICP piles' first time static tests.
387 In both cases ten cycles were imposed with Q_{cyc}/Q_t of ≈ 0.3 and Q_{mean}/Q_t of ≈ 0.4 where Q_t was the
388 earlier static tension failure load. The levels were increased to Q_{cyc}/Q_t of ≈ 0.4 and Q_{mean}/Q_t of 0.45
389 for ICP01 and 0.5 for ICP02 for a second set of 10 cycles. Jardine and Standing (2012) and Rimoy *et al.*
390 (2013) applied working definitions in their interpretation of open-ended tube piles driven in dense
391 sand at Dunkirk. Stable cyclic loading was characterised as showing low and stabilising accumulated

392 displacements, with no failure observed after >1000 cycles. Unstable cycling was defined by significant
393 displacement accumulation and failure within 100 cycles. Metastable intermediate behaviour was
394 recognised in cases where displacements accumulated, without stabilising, leading to failure or
395 degradation in operational capacity between 100 and 1000 cycles. Figure 19 shows the evolution of
396 accumulated permanent displacement, s_{acc} under cycling, indicating either metastable or unstable
397 responses in terms of these cyclic definitions, considering cases where the maximum shaft loads
398 ($Q_{cyc} + Q_{mean}$) amounted to 0.7 to 0.9 times Q_t .

399 Following the end of cycling, ICP02 was unloaded and subjected to a static tension test to failure that,
400 as shown on Figure 15, indicated a 13% capacity loss. A further 4% loss of capacity would have been
401 required to reach failure in this $Q_{max}/Q_t \approx 0.82$ test, which might have been achieved within tens of
402 cycles if the experiments had continued. Overall, the piles did not appear to be unduly sensitive to
403 high level one-way cycling, as was seen in the cyclic tests on driven piles reported by Buckley *et al.*
404 (2017), who warn that the effects of high level two-way axial cycling are likely to be more severe.

405 The SST instruments also revealed the local shaft stress response to cyclic loading. As demonstrated
406 in Figure 20, cycling invoked a similar shear and radial effective stress response to that under static
407 loading. The effective stress path gradients led to σ'_r rising as τ_{rz} was applied in each cycle and also
408 drifting as cycling continued. Comparison of the σ'_r measurements made on unloading after i) static
409 testing and ii) cyclic testing indicated overall σ'_r reductions of up to 29% for ICP02, while ICP02
410 indicated a 5% reduction at the *leading* instrument and an increase of 27% at the *following* instrument,
411 as indicated by points B and C on Figure 20. Very little change in pore pressure was observed during
412 cycling at the rate applied (1 per minute) and the substantially drained response observed is
413 compatible with the consolidation analyses discussed previously.

414 SUMMARY & CONCLUSIONS

415 The mechanical behaviour of piles driven in chalk is poorly understood, leading to considerable
416 uncertainty in foundation design, especially for large offshore wind farms. A field programme in low-
417 medium density chalk with highly instrumented jacked field model pile tests has allowed new insights
418 into aspects of displacement pile behaviour in these problematic geomaterials. The main conclusions
419 are:

- 420 1. Base resistance varied directly with local cone resistance and depended on drainage
421 conditions;
- 422 2. Shaft resistances are low during installation, with the jacked piles' average values exceeding
423 those back analysed from open ended piles driven at the same site;
- 424 3. Large excess pore water pressure are interpreted as having developed under the pile tip
425 during penetration that dissipated rapidly as the tip advanced;
- 426 4. Low stationary radial effective stresses developed during installation that correlated directly
427 with net cone resistance, showing ratios to q_t comparable to those in calcareous sands;
- 428 5. Strong total radial reductions in shaft radial effective stresses, σ'_{rm} develop immediately after
429 the pile tip passes any given horizon, with more gentle additional degradation applying further
430 along the shaft. Still more reductions in σ'_{rm} with relative tip depth (h/R) apply to driven piles;
- 431 6. The effective stress paths recorded during static and cyclic loading tests show that shaft failure
432 is controlled by a Coulomb law, with an interface shear angle similar to that mobilised in
433 laboratory interface ring shear tests. The radial effective stresses rise under static loading until
434 interface dilation reaches its limit. The degree of radial expansion experienced at the interface
435 appears to be far smaller than with sands, due to the higher ratio between the pile roughness
436 and the silt sized crushed chalk grain size;
- 437 7. Long term monitoring of the jacked piles showed total shaft radial stresses reducing with time
438 after installation, falling by 11 to 34% after 23 and 80 days respectively. Tension load tests

439 showed shaft capacity reducing by similar proportions over the weeks that follow installation,
440 in marked contrast with the strong set up shown by open driven piles at the same site;

441 8. Geometry and/or installation method influence the ageing and subsequent loading
442 behaviours and require further investigation;

443 Nevertheless, conclusions 1 to 6 are fully compatible with observations made at the same site with
444 open-ended driven piles, which developed far higher capacities than are recommended by the current
445 CIRIA guidelines. The ICP tests provide key insights that will help guide new, more fundamental and
446 reliable, effective stress based design methods for piles driven in chalk.

447 **ACKNOWLEDGEMENTS**

448 This study is part of a joint industry project led by Mr. Pedro Barbosa that is funded by Innovate UK
449 (formerly the Technology Strategy Board), Iberdrola/Scottish Power Renewables and supported by
450 the Geotechnical Consulting Group, London represented by Dr. Felix Schroeder. The Authors
451 acknowledge the help of Dr. Jit Kheng Lim and Tom Pine from University of Western Australia and Emil
452 Ushev and Tingfa Liu of Imperial College who helped to conduct the pile tests. The Authors also
453 acknowledge the support of Lankelma Ltd, Iden, East Sussex in carrying out this work.

REFERENCES

- Baligh M. M. (1985). Strain path method. *J. Geotech. Eng-ASCE*, **111**, No. 9, 1108-1136.
- Barbosa P., Geduhn, M., Jardine, R. J., Schroeder, F. C. & Horn, M. (2015). Offshore pile load tests in chalk. In: *Proc. 16th Eur. Conf. Soil Mech. & Geotech. Eng.*, Edinburgh, Scotland, pp. 2885-2890
- Bialowas G., Diambra, A. & Nash, D. (2016). Small strain stiffness evolution of reconstituted medium density chalk. In: *Proc. 1st IMEKO TC4 Intl. Workshop on Metrology for Geotechnics*, Benevento, Italy, pp.
- Bond A. J. (1989). *Behaviour of displacement piles in overconsolidated clays*. PhD Thesis, Imperial College London (University of London), London, UK
- Bond A. J., Jardine, R. J. & Dalton, J. C. P. (1991). Design and performance of the Imperial College instrumented pile. *Geotech. Test. J.*, **14**, No. 4, 413-424.
- Boulon M. & Foray, P. (1986). Physical and numerical simulation of lateral shaft friction along offshore piles in sand. In: *Proc. 3rd Intl Conf. on Numerical methods in offshore piling*, Nantes, France, pp. 127-147
- Bowden A. J., Spink, T. W. & Mortimore, R. N. (2002). The engineering description of chalk: its strength, hardness and density. *Q. J. Eng. Geol. Hydrogeol.*, **35**, No. 4, 355-361.
- Buckley R. M., Jardine, R. J., Kontoe, S., Parker, D. & Schroeder, F. C. (2017). Ageing and cyclic behaviour of axially loaded piles driven in chalk. *Géotechnique*, No. <https://doi.org/10.1680/jgeot.17.P.012>.
- Bundy S. P. S. (2013). *Geotechnical properties of chalk putties*. PhD Thesis, University of Portsmouth, Portsmouth, UK
- Carrington T. M., Li, G. & Rattley, M. J. (2011). A new assessment of ultimate unit friction for driven piles in low to medium density chalk. In: *Proc. 15th Eur. Conf. Soil Mech. & Geotech. Eng.*, Amsterdam, The Netherlands, pp. 825-830
- Cassidy M. J. (2012). Experimental observations of the penetration of spudcan footings in silt. *Géotechnique*, **62**, No. 8, 727-732.
- Chan L. D. (2017). *Laboratory investigation of chalk-steel interface shearing*. MSc Thesis,
- Chen L. D. (2017). *Laboratory investigation of chalk-steel interface testing*. MSc Thesis, Imperial College, London
- Chow F. C. (1997). *Investigations into Displacement Pile Behaviour for Offshore Foundations*. PhD Thesis, Imperial College London, London, UK
- Chung S. F., Randolph, M. F. & Schneider, J. A. (2006). Effect of penetration rate on penetrometer resistance in clay. *J. Geotech. Geoenviron. Eng.*, **132**, No. 9, 1188-1196.
- Ciavaglia F., Carey, J. & Diambra, A. (2017). Time-dependent uplift capacity of driven piles in low to medium density chalk. *Géotechnique Letters* 7. March, 1-7
- Clayton C. J. (1986). The chemical environment of flint formation in Upper Cretaceous chalks. In: *Proc. 4th Int. Flint. Symp. The scientific study of flint and chert*, Brighton, UK, pp. 43-54
- Clayton C. R. I., Matthews, M. C. & Heymann, G. (2002). The Chalk. In: *Proc. 1st Intl. Workshop on Characterisation and Engineering Properties of Natural Soils*, Singapore, pp. 1403-1434

- Diambra A., Ciavaglia, F., Dimelow, C., Carey, J. & Nash, D. F. T. (2014). Performance of cyclic cone penetration tests in chalk. *Géotechnique Letters* 4. July–September, 230-237
- Doughty L. (2016). *Laboratory testing of chalk*. MSc Thesis, Imperial College London, London, UK
- Dührkop J., Augustesen, A. H. & Barbosa, P. (2015). Cyclic pile load tests combined with laboratory results to design offshore wind turbine foundations in chalk. In: *Proc. Conf. Frontiers in Offshore Geotechnics III (ISFOG)*, Oslo, Norway, pp. 533-538
- Fahey M. & Lee Goh, A. (1995). A comparison of pressuremeter and piezocone methods of determining the coefficient of consolidation. In: *Proc. 4th Intl. Symp. on the Pressuremeter and Its New Avenues*, Quebec, Canada, pp. 153-60
- Finnie I. M. S. & Randolph, M. F. (1994). Punch-through and liquefaction induced failure of shallow foundations on calcareous sediments. In: *Proc. Int. Conf. Behavior of Offshore Structures*, Boston, Massachusetts, pp. 217-230
- Fugro (2012a). *Laboratory testing report: Pile test site, chalk specific testing. St. Nicholas at Wade, UK, D34001-2*.
- Fugro (2012b). *Onshore geotechnical report: field data St. Nicholas at Wade UK, D34001-1*.
- Hobbs N. B. & Atkinson, M. S. (1993). Compression and tension tests on an open-ended tube pile in chalk. *Ground Engineering*, **26**, No. 3, 31-34.
- Hodges W. G. H. & Pink, S. (1971). The use of penetrometer soundings in the estimation of pile bearing capacity and settlement for driven piles in highly weathered chalk in Portsmouth areas as an alternative to site investigation by borehole sampling and laboratory testing. In: *Proc. Roscoe. Mem. Symp.: Stress strain behaviour of soils*, Cambridge University, pp. 769-774
- Jardine R. J., Symes, M. J. & Burland, J. B. (1984). The measurement of soil stiffness in the triaxial apparatus. *Géotechnique*, **34**, No. 3, 323-340.
- Jardine R. J., Chow, F. C., Overy, R. & Standing, J. R. 2005. *ICP design methods for driven piles in sands and clays*, London: Thomas Telford.
- Jardine R. J. & Standing, J. R. (2012). Field axial cyclic loading experiments on piles driven in sand. *Soils Found.*, **52**, No. 4, 723-736.
- Jardine R. J., Zhu, B. T., Foray, P. & Yang, Z. X. (2013). Interpretation of stress measurements made around closed-ended displacement piles in sand. *Géotechnique*, **63**, No. 8, 613-627.
- Jardine R. J. (2018). Geotechnics and Energy: 56th Rankine Lecture. *Géotechnique*, to appear.
- Kishida H. & Uesugi, M. (1987). Tests of the interface between sand and steel in the simple shear apparatus. *Géotechnique*, **37**, No. 1, 45-52.
- Le T. M. H., Eiksund, G. R., Strøm, P. J. & Saue, M. (2014). Geological and geotechnical characterisation for offshore wind turbine foundations: A case study of the Sheringham Shoal wind farm. *Engineering Geology*. 2014, 40-53
- Lehane B. M. & Jardine, R. J. (1992). The behaviour of a displacement pile in Bothkennar clay. In: *Proc. Wroth Memorial Symp. on Predictive Soil Mechanics*, Oxford, UK, pp. 421-435
- Lehane B. M. (1992). *Experimental Investigations of Pile Behaviour using Instrumented Field Piles*. PhD Thesis, Imperial College London,
- Lehane B. M., Jardine, R. J., Bond, A. J. & Frank, R. (1993). Mechanisms of shaft friction in sand from instrumented pile tests. *J. Geotech. Eng-ASCE*, **119**, No. 1, 19-35.
- Lehane B. M., Schneider, J. A. & Xu, X. (2005). *A review of design methods for offshore driven piles in siliceous sand*, UWA Report 05358.

- Lehane B. M., Schneider, J. A., Lim, J. K. & Mortara, G. (2012). Shaft friction from instrumented displacement piles in an uncemented calcareous sand. *J. Geotech. Geoenviron. Eng.*, **138**, No. 11, 1357-1368.
- Lings M. L. & Dietz, M. S. (2005). The peak strength of sand-steel interfaces and the role of dilation. *Soils Found*, **45**, No. 6, 1-14.
- Lord J. A., Twine, D. & Yeow, H. 1994. *Foundations in chalk Report PR11*, London, UK: CIRIA.
- Lord J. A., Clayton, C. R. I. & Mortimore, R. N. 2002. *Report C574: Engineering in chalk*, London, UK: CIRIA.
- Met-Office (2016). Daily and hourly rainfall datasets from weather station at Manston 30 September 2015 - 14 February 2016.
- Power P. (1982). The use of the electric static cone penetrometer in the determination of the engineering properties of chalk. In: *Proc. 2nd Eur. Symp. on Penetration Testing*, Amsterdam, The Netherlands, pp. 769-774
- Randolph M. F., Dolwin, J. & Beck, R. (1994). Design of driven piles in sand. *Géotechnique*, **44**, No. 3, 427-48.
- Randolph M. F. (2004). Characterisation of soft sediments for offshore applications. In: *Proc. 2nd Int. Conf. on Site Characterisation*, Porto, Portugal, pp. 209-232
- Rimoy S. P., Jardine, R. J. & Standing, J. R. (2013). Displacement response to axial cycling of piles driven in sand. *Proc. of the ICE Geotech. Eng.*, **166**, No. GE2, 131-146.
- Setech (2007). *Trial site investigation - Thanet offshore wind farm trial site*, 8564/1.
- Suzuki Y. (2014). *Investigation and interpretation of cone penetration rate effects*. PhD Thesis, The University of Western Australia, Crawley, Australia
- Teh C. I. & Houlsby, G. T. (1991). An analytical study of the cone penetration test in clay. *Géotechnique*, **41**, No. 1, 17-34.
- Yang Z. X., Jardine, R. J., Zhu, B. T., Foray, P. & Tsuha, C. H. C. (2010). Sand grain crushing and interface shearing during displacement pile installation in sand. *Géotechnique*, **60**, No. 6, 469-482.
- Ziogos A., Brown, M., Ivanovic, A. & Morgan, N. (2016). Chalk-steel interface testing for marine energy foundations. *Proc. of the ICE Geotech. Eng.* DOI: 10.1680/jgeen.16.00112. 0, 1-14

NOTATION

Roman Alphabet

c'	Cohesion intercept
c_h	Coefficient of horizontal consolidation
$c_{h,NC}$	Coefficient of horizontal consolidation under normally consolidated conditions
$c_{h,OC}$	Coefficient of horizontal consolidation under overconsolidated conditions
$c_{h,piezo}$	Operational coefficient of horizontal consolidation during PCPT dissipation tests
D	Diameter of pile or penetrometer
D_{50}	Mean particle size
f_s	PCPT sleeve friction
G_{hv}	Shear modulus measured during cross hole seismic tests
G_{vh}	Shear modulus measured during seismic CPT
h	Distance from the pile tip
k_l	Cyclic loading stiffness
k_s	Displacement creep rate
N	Number of cycles
q_b	Base resistance
q_c	PCPT cone resistance
q_t	Net PCPT cone resistance
Q_b	Pile base capacity
Q_{cyc}	Axial cyclic load amplitude
Q_{mean}	Mean axial cyclic load
Q_{tot}	Total pile capacity in compression
Q_t	Current pile shaft capacity in tension
$Q_{t(EoD)}$	Static compressive tension capacity at EoD from dynamic tests
Q_u	Ultimate equalised pile capacity in tension
R	Pile radius
RR	Relative roughness
R_{cla}	Average centre line roughness
s_{acc}	Accumulated permanent cyclic displacement
t	Time
t_{50}	Time for 50% dissipation of excess pore water pressures in a PCPT dissipation test
u_a	PCPT pore pressure measured at the u_a position
u_2	PCPT pore pressure measured at the u_2 position
v	Velocity of the pile or penetrometer
V	Dimensionless velocity
V_{pile}	Dimensionless velocity of the pile

V_{CPT}

Dimensionless velocity of the PCPT

Greek alphabet

α	Parameter to describe relationship between q_b and q_t
δ_{CPT}	Interface angle applying on PCPT shaft
δ_f	Interface friction angle at failure
δ_{cv}	Constant volume interface friction angle
σ_r	Radial total stress
σ'_{rc}	Radial effective stress after equalisation
σ'_{rf}	Radial effective stress at failure
σ'_{rm}	Maximum penetration radial effective stress
σ'_{rs}	Stationary radial effective stress
σ_z	Vertical stress beneath the pile tip
σ_1	Principal effective stress
$\Delta\sigma'_{rd}$	Dilative component during loading
τ_{avg}	Average installation compressive shaft resistance
τ_f	Local shear stress at failure
$\tau_{s,EoD}$	Average shear stress along pile length at the end of driving
$\tau_{s,Eoj}$	Average shear stress along pile length at the end of jacking
τ_{rz}	Local shear stress
φ'	Effective angle of shearing resistance

LIST OF FIGURES

Figure 1 Site plan a) showing site b) ICP jacked instrumented pile tests and driven piles reported by Buckley et al. (2017)

Figure 2 Particle size distribution of samples of crushed chalk from the site

Figure 3 Cone penetration tests used in the analysis of jacked pile test results

Figure 4 ICP configuration used during tests in chalk a) ICP01 b) ICP02

Figure 5 Schematic of test rig (not to scale) a) side view b) elevation (after Buckley et al, 2017)

Figure 6 Load controlled cyclic loading pattern and cyclic loading conventions

Figure 7 Force at the pile head during installation (Q_{tot}) force at the pile base (Q_b), average shear stress over the pile length (τ_{avg}) and envelope of q_c measurements

Figure 8 Variation in excess pore water pressure with normalised distance from the tip during PCPT and jacked pile penetration. Note initial pre installation pore pressures are small or negative

Figure 9 Variation in alpha value with normalised velocity for the jacked pile and PCPT

Figure 10 Profiles of SST measurements at the leading instrument during pauses in jacking a) stationary local radial effective stresses b) stationary local shear stresses

Figure 11 Relationship between cone resistance and stationary radial effective stress at the leading instrument

Figure 12 a) normalised stationary radial effective stresses along the pile shaft during installation compared to historical measurements b) normalised stationary and moving radial effective stresses from SST measurements, CPT f_s readings and back analysis of dynamic test data on driven piles

Figure 13 Typical short term changes in local radial effective stress, local shear stress and pore water pressure

Figure 14 Variation of local effective shaft radial stresses with time over entire equalisation period

Figure 15 Net pile head load versus displacement during static tension and one way cyclic loading on ICP01 and ICP02

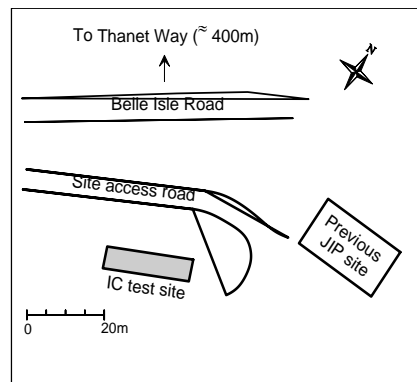
Figure 16 Variation in axial load and average shear stress along the pile length at the point of tension failure

Figure 17 Effective stress paths during static tension loading at a) the leading SST1 and b) the following SST2

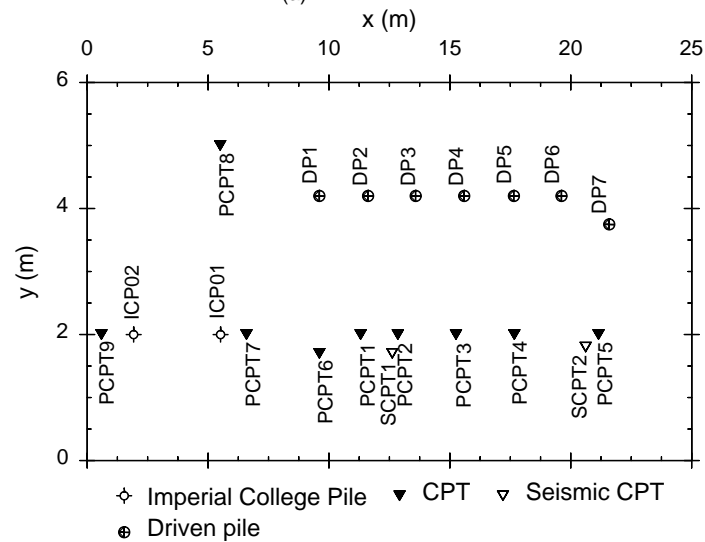
Figure 18 Comparison of set up factors observed following equalisation periods for driven piles from Buckley et al. (2017) (and jacked piles as part of this study)

Figure 19 Evolution of permanent pile head displacement with number of cycles

Figure 20 Effective stress paths during one way cyclic loading at a) leading SST1 during ICP01 b) following SST2 during ICP01 c) leading SST1 during ICP02 d) following SST2 during ICP02



(a)



(b)

Figure 1 Site plan a) showing site b) ICP jacked instrumented pile tests and driven piles reported by Buckley et al. (2017)

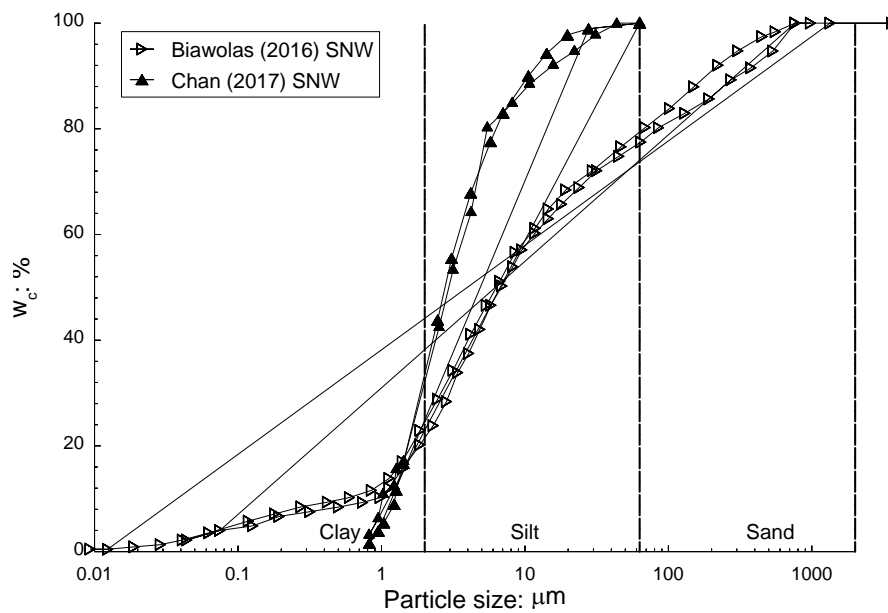


Figure 2 Particle size distribution of samples of crushed chalk from the site

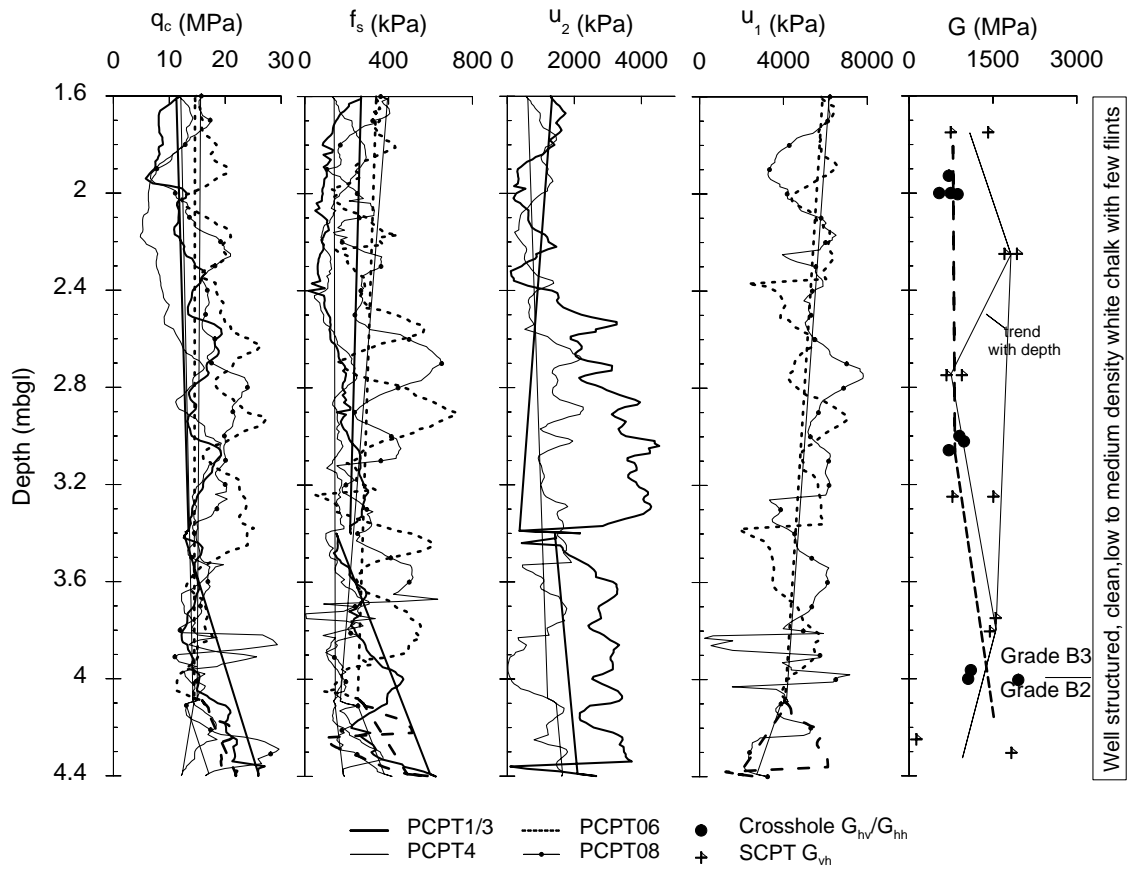


Figure 3 Cone penetration tests used in the analysis of jacked pile test results

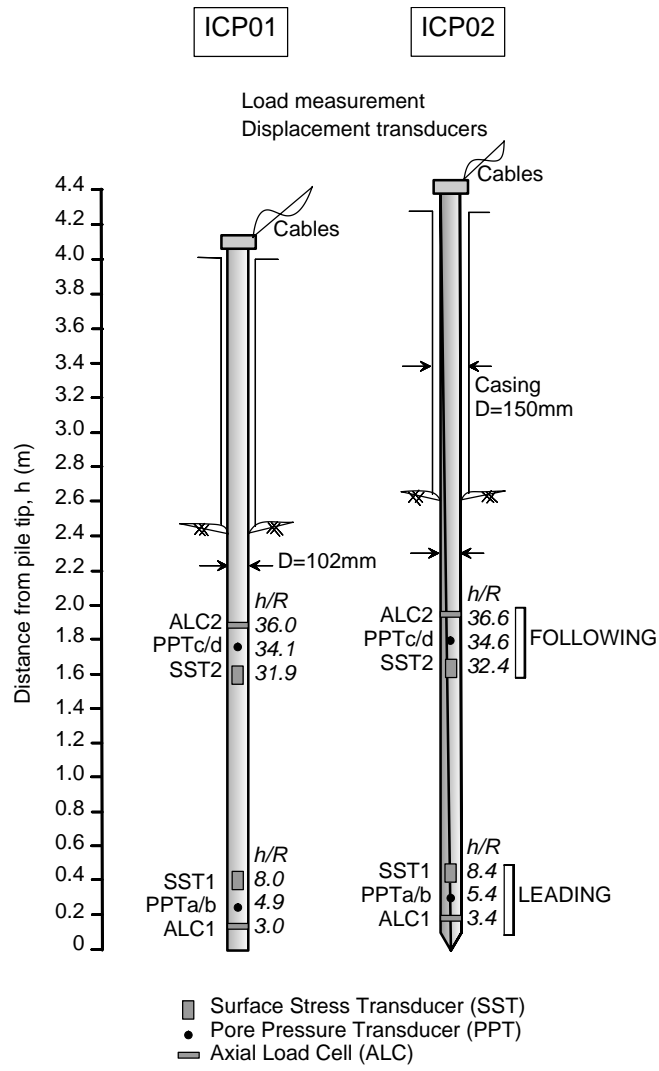


Figure 4 ICP configuration used during tests in chalk a) ICP01 b) ICP02

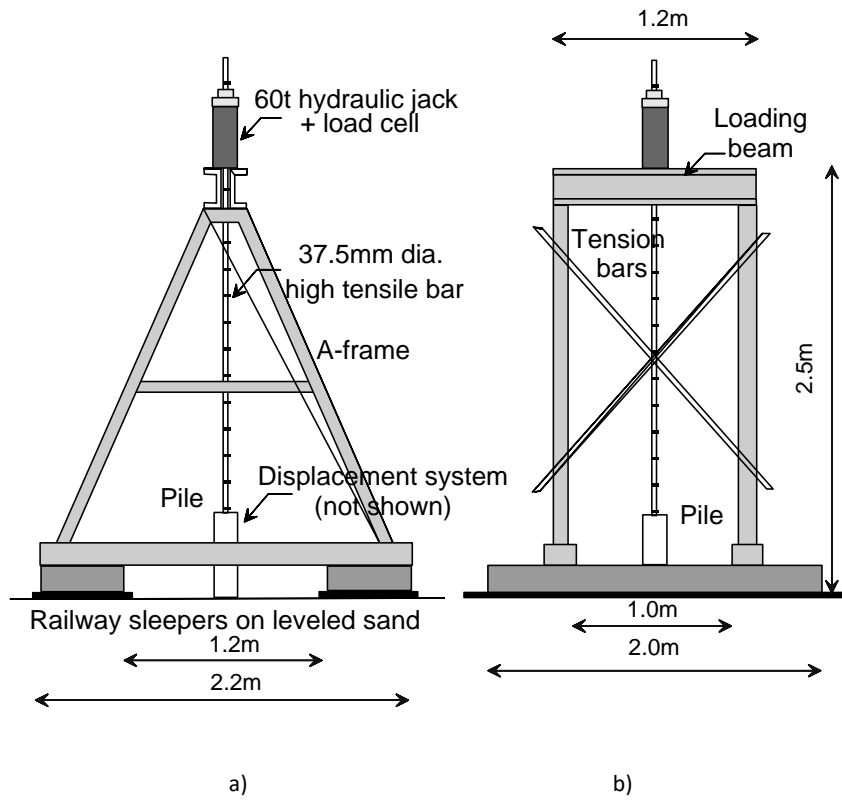


Figure 5 Schematic of test rig (not to scale) a) side view b) elevation (after Buckley et al, 2017)

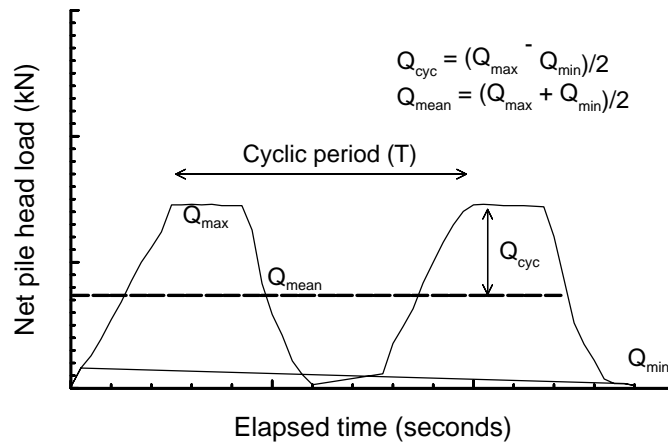


Figure 6 Load controlled cyclic loading pattern and cyclic loading conventions

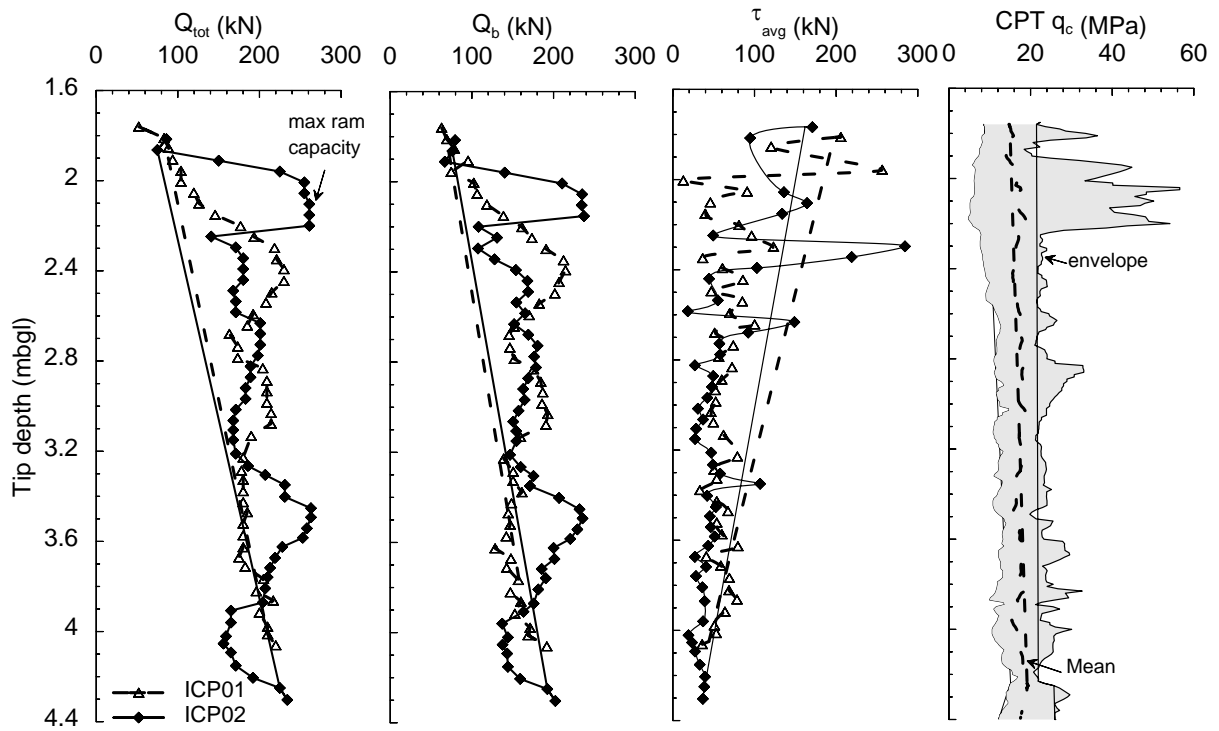


Figure 7 Force at the pile head during installation (Q_{tot}) force at the pile base (Q_b), average shear stress over the pile length (τ_{avg}) and envelope of q_c measurements

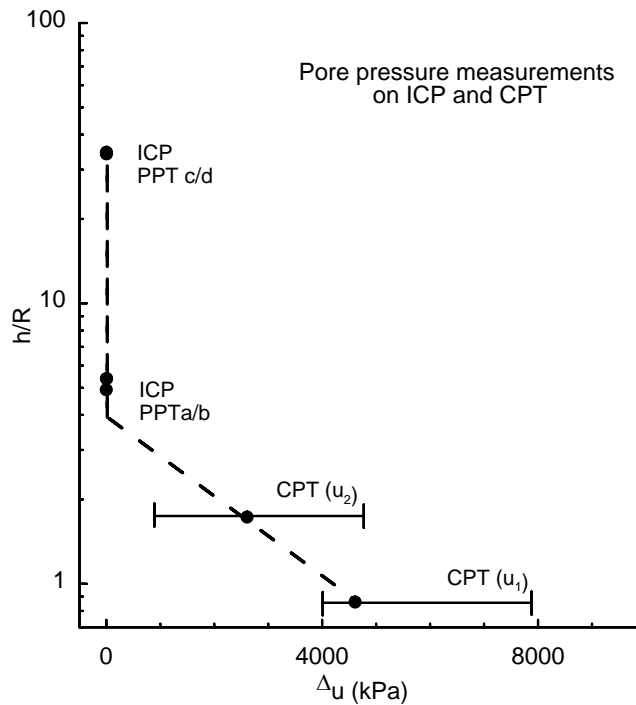


Figure 8 Variation in excess pore water pressure with normalised distance from the tip during PCPT and jacked pile penetration. Note initial pre installation pore pressures are small or negative

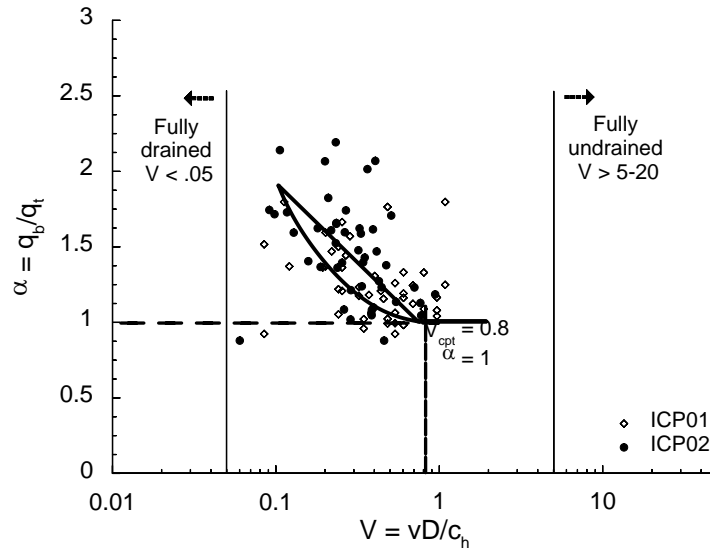


Figure 9 Variation in alpha value with normalised velocity for the jacked pile and PCPT

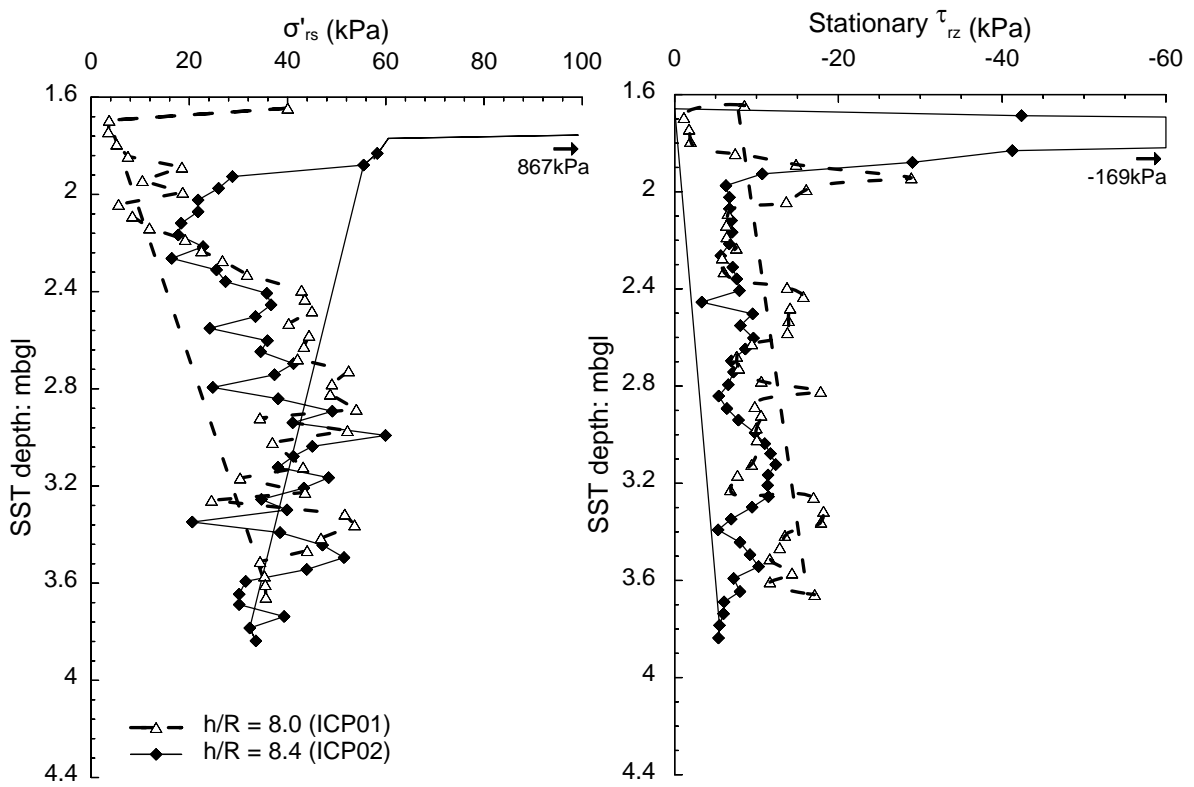


Figure 10 Profiles of SST measurements at the leading instrument during pauses in jacking a) stationary local radial effective stresses b) stationary local shear stresses

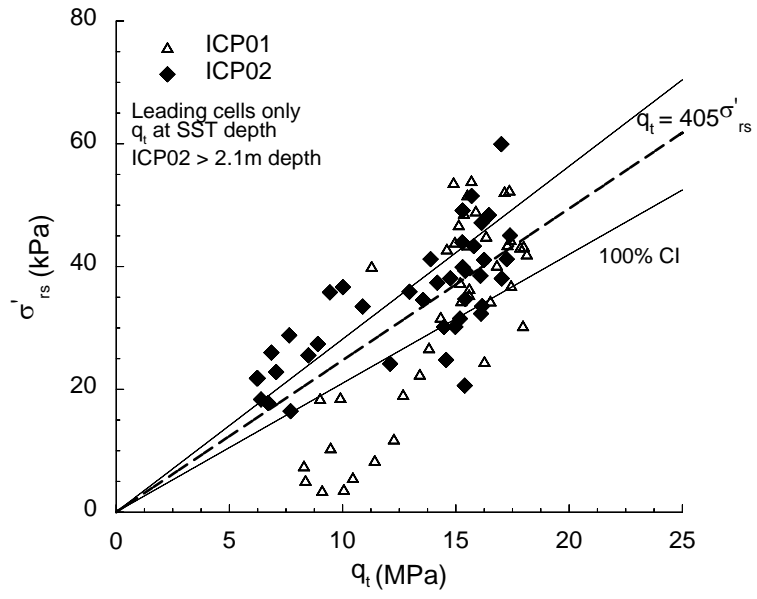
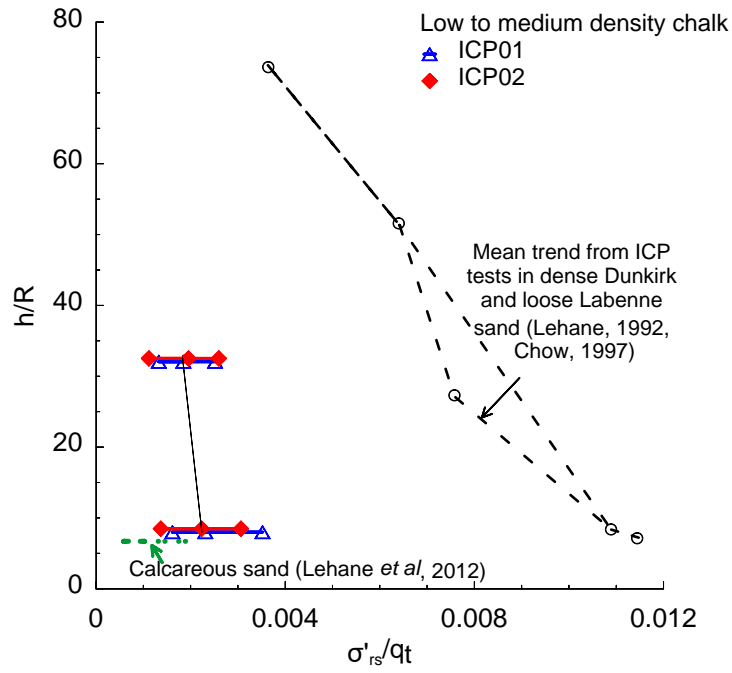
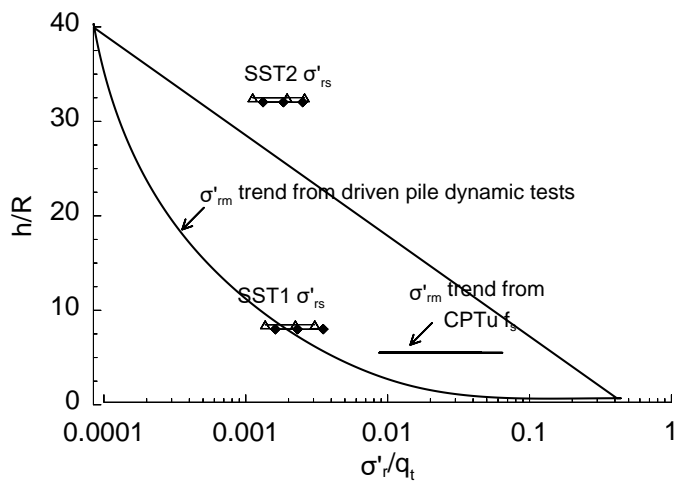


Figure 11 Relationship between cone resistance and stationary radial effective stress at the leading instrument



(a)



(b)

Figure 12 a) normalised stationary radial effective stresses along the pile shaft during installation compared to historical measurements b) normalised stationary and moving radial effective stresses from SST measurements, CPT f_s readings and back analysis of dynamic test data on driven piles

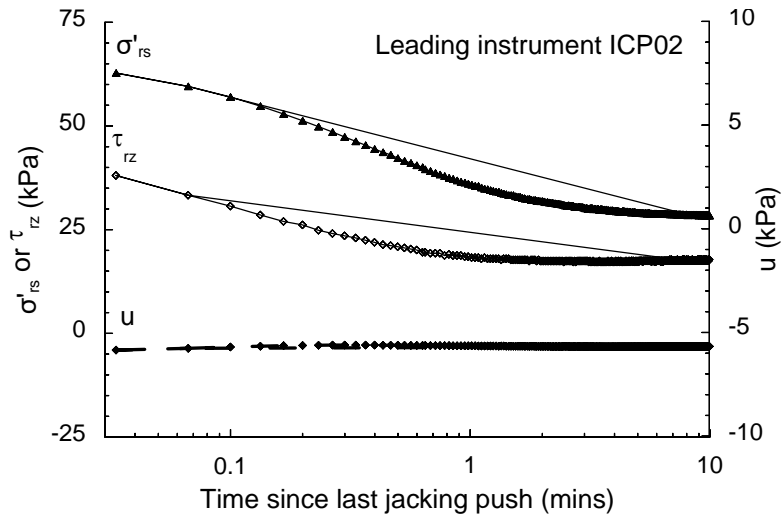


Figure 13 Typical short term changes in local radial effective stress, local shear stress and pore water pressure

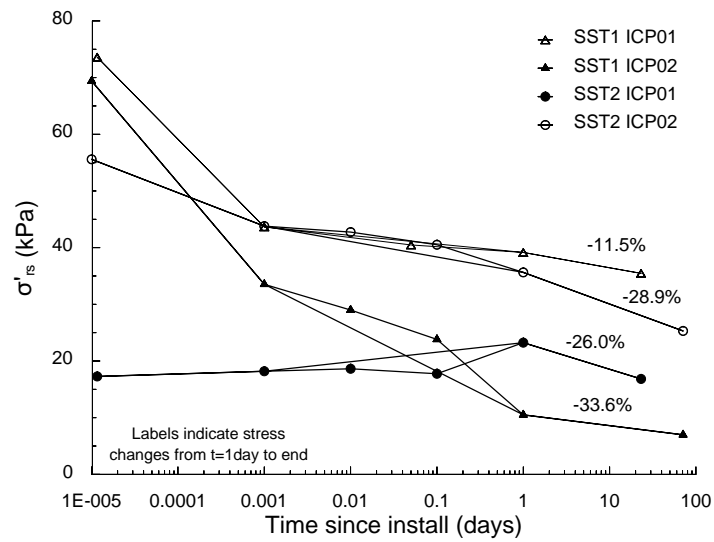


Figure 14 Variation of local effective shaft radial stresses with time over entire equalisation period

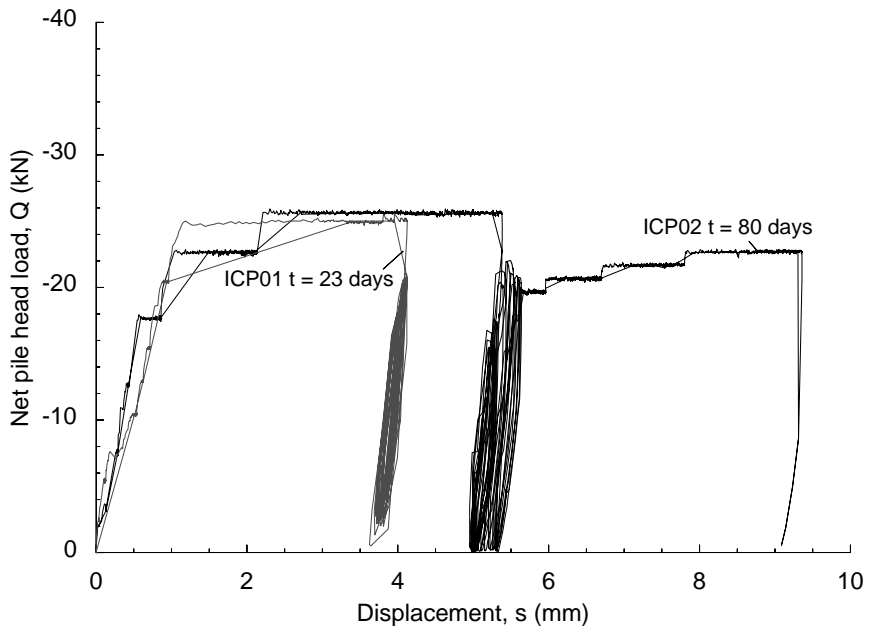


Figure 15 Net pile head load versus displacement during static tension and one way cyclic loading on ICP01 and ICP02

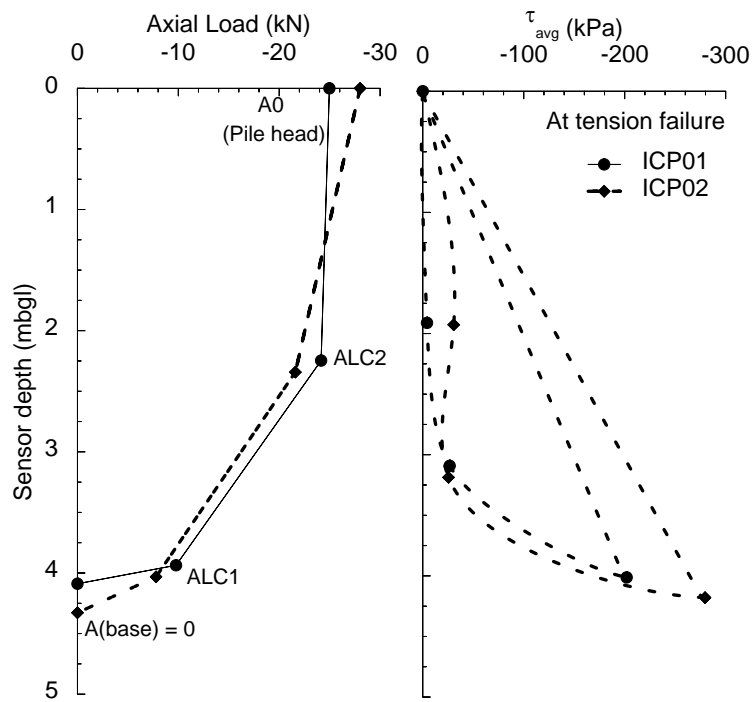


Figure 16 Variation in axial load and average shear stress along the pile length at the point of tension failure

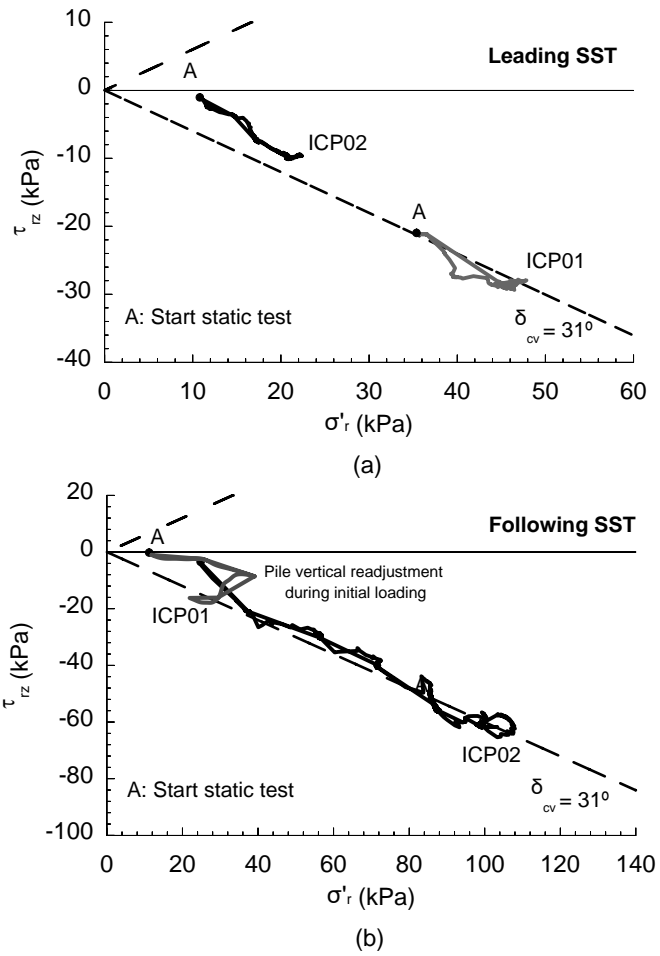


Figure 17 Effective stress paths during static tension loading at a) the leading SST1 and b) the following SST2

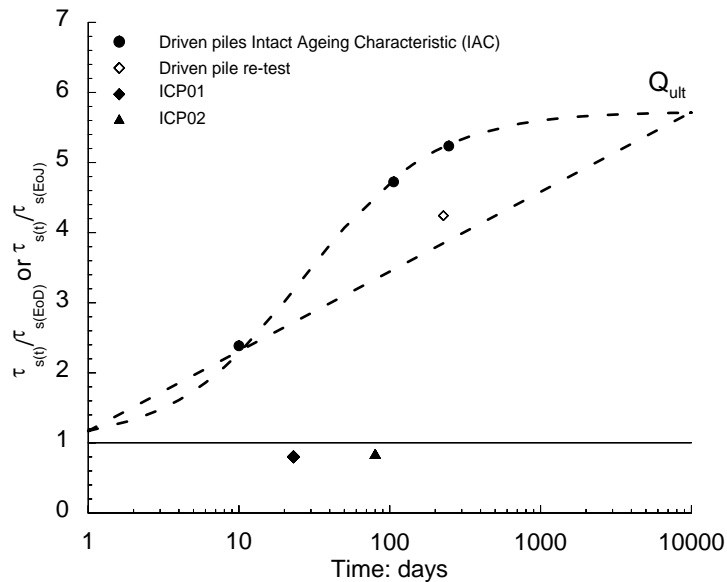


Figure 18 Comparison of set up factors observed following equalisation periods for driven piles from Buckley et al. (2017) (and jacked piles as part of this study)

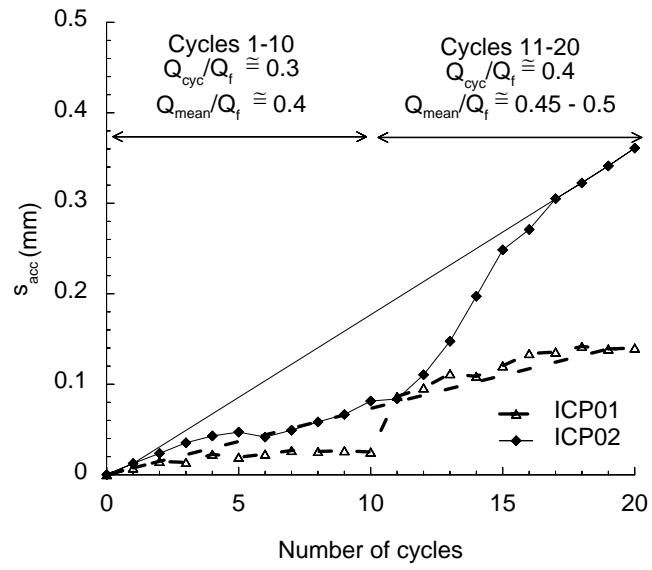
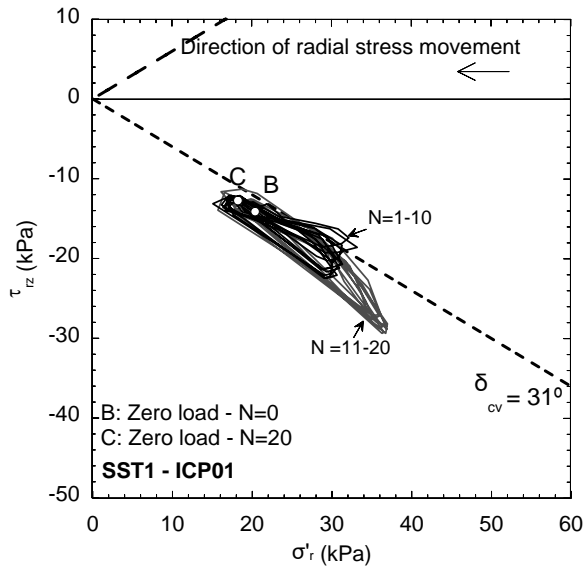
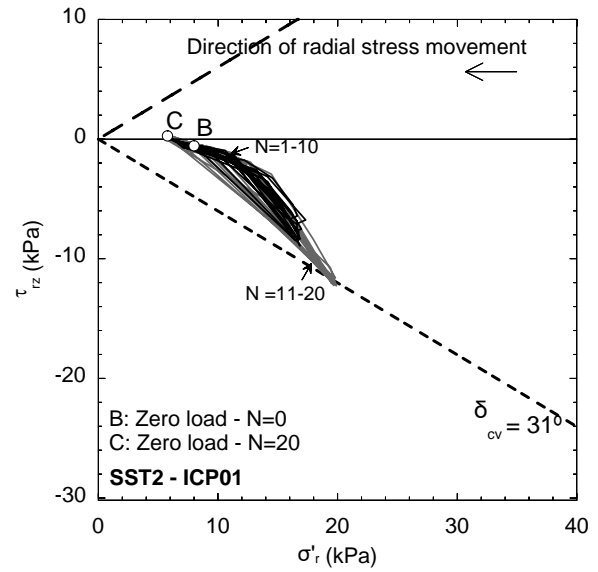


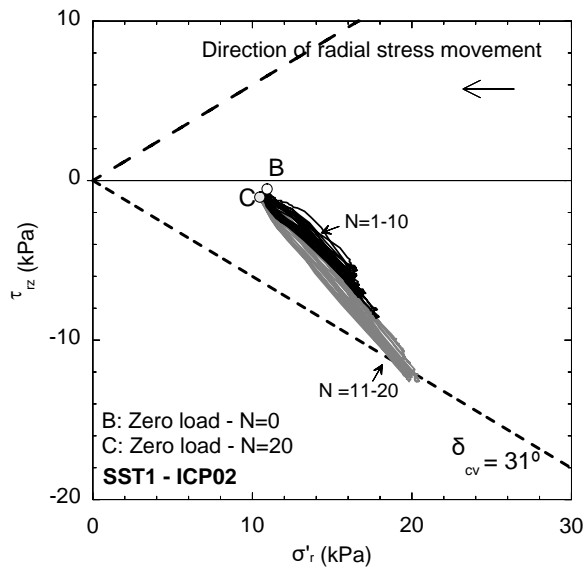
Figure 19 Evolution of permanent pile head displacement with number of cycles



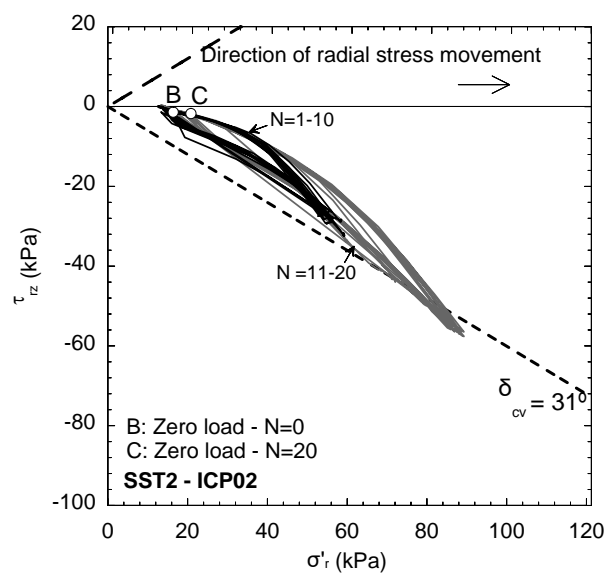
(a)



(b)



(c)



(d)

Figure 20 Effective stress paths during one way cyclic loading at a) leading SST1 during ICP01 b) following SST2 during ICP01 c) leading SST1 during ICP02 d) following SST2 during ICP02

Table 1 Summary of 102mm diameter ICP test programme

Test	ICP01	ICP02
End condition	Flat base	Conical tip
Number of installation jacking cycles	51	56
Average dimensionless velocity, V_{pile}	0.46	0.33
Final Penetration (mbgl)	4.09	4.33
Length of embedment (m)	2.49	2.73
L/D	24.4	26.8
Installation date	27/10/2015	21/11/2015
First tension test date	19/11/2015	09/02/2016
Ageing period (days)	23	80